HT2009-88212

REAL-TIME RELIABLE SIMULATION OF HEAT TRANSFER PHENOMENA

G. Rozza[*]
Modelling and Scientific Computing, CMCS
Ecole Polytechnique Fédérale de Lausanne, EPFL
Station 8-MA, Lausanne
CH-1015, Switzerland
Email: gianluigi.rozza@epfl.ch
MIT research affiliate

D. B. P. Huynh
Department of Mechanical Engineering,
National University of Singapore,
21, Lower Kent Ridge Road
119077, Singapore
Email: baophuonghk@gmail.com
SMA, Singapore-MIT Alliance

N. C. Nguyen
Department of Aeronautics and Astronautics,
Massachusetts Institute of Technology, MIT,
Room 37-435, 77 Massachusetts Avenue,
Cambridge, MA 02139, US
Email: cuongng@mit.edu

A.T. Patera
Department of Mechanical Engineering,
Massachusetts Institute of Technology, MIT,
Room 3-266, 77 Massachusetts Avenue,
Cambridge, MA 02139, US
Email: patera@mit.edu

ABSTRACT

In this paper we discuss the application of the certified reduced basis method and the associated software package rbMIT© to "worked problems" in steady and unsteady conduction. Each worked problem is characterized by an input parameter vector — material properties, boundary conditions and sources, and geometry — and desired outputs — selected fluxes and temperatures. The methodology and associated rbMIT© software, as well as the educational worked problem framework, consists of two distinct stages: an Offline (or "Instructor") stage in which a new heat transfer worked problem is first created; and an Online (or "Lecturer"/"Student") stage in which the worked problem is subsequently invoked in (say) various in–class, project, or homework settings. In the very inexpensive Online stage, given an input parameter value, the software returns both (i) an accurate reduced basis output prediction, and (ii) a rigorous bound for the error in the reduced basis prediction relative to an underlying expensive high-fidelity finite element dis-cretization; as required in the educational context, the response is both rapid and reliable. We present illustrative results for two worked problems: a steady thermal fin, and unsteady thermal analysis of a delamination crack.

Keywords Reduced basis method, error bounds, real-time computation, steady and unsteady heat transfer, parametrized systems, educational worked problems.

1 INTRODUCTION

There are many examples of numerical simulation in heat transfer education [7, 15–18, 21]. However, classical approaches, such as the finite element method, are often too slow; and more *ad hoc* procedures, such as low-order heuristic models, are often unreliable. Our goal is to achieve the accuracy and reliability of a high-fidelity approximation but at the greatly reduced cost of a low-order model. The resulting pedagogical prospects are very attractive: *interactive* in-class visualizations and parametric exploration; rapid assessment of (classical) engineering approximations and interpretations (from thermal fins to boundary layers

---

[*]Corresponding Author

to lumped models); and incorporation of more realistic examples in homework assignments and design projects.

Our approach is built upon the certified reduced basis method [10, 13, 19] for rapid and reliable prediction of engineering outputs associated with parametrized partial differential equations. In particular, we consider a (say, single) "output of interest" $s \in \mathbb{R}$ – related to temperatures or fluxes – as a function of an "input parameter" P-vector $\boldsymbol{\mu}$ – related to geometry, physical properties, boundary conditions, or sources. The input parameter domain – the set of possible inputs – is denoted $\mathcal{D}$, which is a subset of $\mathbb{R}^P$.

The output of interest $s(\boldsymbol{\mu})$ is a (say, linear) functional ℓ of a field variable $u(\boldsymbol{\mu})$, $s(\boldsymbol{\mu}) = \ell(u(\boldsymbol{\mu}))$. Here $u(\boldsymbol{\mu})$ – in our case the temperature – satisfies a partial differential equation parametrized with respect to $\boldsymbol{\mu}$. We thus arrive at an input-output statement $\boldsymbol{\mu} \to s(\boldsymbol{\mu})$ evaluation of which requires solution of a parametrized partial differential equation. We consider partial differential equations for which the parametric dependence is strictly or approximately affine; "affine" dependence implies that the parametrized differential operator can be expressed as a sum of Q products of [parameter-dependent functions] × [parameter-independent operators].

As regards "rapid," our method minimizes the marginal cost associated with (approximate) input-output evaluation, and is thus most useful either (a) in the real-time or interactive context, or (b) in the limit of many queries. Engineering situations which satisfy these criteria include in-the-field robust parameter estimation (or inverse problems, or nondestructive evaluation), design and optimization, and control. Many educational situations also satisfy these criteria – from in-class demonstrations that require extensive parameter exploration and immediate gratification to homework assignments and projects that must be completed (by many parties) rapidly on modest platforms.

As regards "reliable," we provide certificates of fidelity with every prediction: an estimate that rigorously bounds the error in our (rapid, approximate) input-output evaluation or field variable relative to a highly accurate (and hence very expensive) "truth" finite element solution $u^{\mathcal{N}}$. In many engineering situations, the certainty provided by these error bounds is crucial. For example, in the real-time context, critical decisions must be made in the field – quickly, without recourse to extensive Offline resources – that are at least feasible and safe if not optimal. Educational situations also demand certainty: a demonstration or project founded upon a-physical numerical artifacts is obviously anathema to the development of sound engineering principles and practices.

The essential components of our approach are threefold.

(i) Rapidly convergent global reduced basis (RB) approximations [1,11] – (Galerkin) projection onto a space $W_N^{\mathcal{N}}$ spanned by solution of the governing partial differential equation at N (optimally) selected points S_N in the parameter set $\mathcal{D}$. Typically, N will be small, as we focus attention on the (smooth) low-dimensional parametrically-induced manifold of interest. The RB approximations to the field variable and output are denoted $u_N(\boldsymbol{\mu})$ and $s_N(\boldsymbol{\mu})$, respectively. Our approach is premised upon a classical Finite Element (FE) method "truth" approximation space of (typically very large) dimension $\mathcal{N}$. It is the FE truth approximation – our $u^{\mathcal{N}}(\boldsymbol{\mu})$ introduced above – upon which we build our RB approximation, and with respect to which we measure the RB error (see (ii) below).

(ii) Rigorous a posteriori error estimation procedures – relaxations of the error-residual equation that provide inexpensive yet sharp bounds for the error in the RB field-variable approximation, $u_N(\boldsymbol{\mu})$, and output(s) approximation, $s_N(\boldsymbol{\mu})$. Our error indicators are rigorous upper bounds for the error (relative to the FE truth approximation) for all $\boldsymbol{\mu} \in \mathcal{D}$ and for all N; furthermore, in many cases, we can prove that the effectivity of our error estimators – the ratio of the error bound to the true error – is $O(1) - O(10)$. Our inexpensive error estimators also serve though a Greedy procedure [19] to construct the optimal RB samples and spaces which ensure an efficient and well-conditioned RB approximation.

(iii) Offline/Online computational procedures – decomposition stratagems which decouple the generation and projection stages of the RB approximation: very extensive (parameter-independent) pre-processing performed Offline *once* that then prepares the way for subsequent very inexpensive calculations performed Online *for each new input-output evaluation required*. The operation count for the Online stage – in which, given a new parameter value $\boldsymbol{\mu}$, the RB Online Evaluator calculates the RB output and associated error bound (relative to the expensive FE truth approximation) – depends only on N and the parametric complexity of the problem. The Online computational complexity and mathematical stability does not depend on $\mathcal{N}$, the dimension of the underlying "truth" FE approximation space; we may thus consider a highly accurate truth approximation.

The Offline-Online procedure dramatically reduces the marginal cost (or asymptotic average cost) of input–output evaluation: the RB approach is thus very attractive in the real-time context (in which we place a premium on immediate response and hence the Offline effort is largely irrelevant) or the many-query context (in which we require many evaluations and hence the Offline effort is asymptotically negligible).

In order to realize the potential of certified reduced basis methods (in heat transfer education) we have developed and applied the rbMIT© package: the rbMIT© software implements (in Matlab®) both the Offline and Online stages of the reduced basis approach. The Offline component of the rbMIT© software automates the (reduced basis) formulation of the problem and construction of the associated FE discretization (on which the RB approximation is built); identifies an optimal reduced basis space for rapid convergence; and generates all the "data" — related to both RB approximation and associated *a posteriori* error estimator — required for

the Online stage. The Online component of the rbMIT©
software includes two capabilities for probing the solution to
the problem for any given new $\boldsymbol{\mu}$: the RB Online Evaluator
returns (rapidly) both an accurate RB prediction for $s^{\mathcal{N}}$, s_N,
and a certificate of fidelity that rigorously bounds the error
$|s^{\mathcal{N}} - s_N|$; the RB Visualizer both renders the relevant field
variable and provides a rigorous bound for the error $u^{\mathcal{N}} - u_N^{\mathcal{N}}$ (in
a norm that measures both function and derivative)[1]. The open-
source rbMIT© software may be downloaded from the URL
`http://augustine.mit.edu/methodology/metho-`
`dology_rbMIT_System.htm`.

In the educational context, the "Instructor" appeals to
the Offline component to construct a "worked problem"; the
"Lecturer" or "Student" invokes the Online component to
probe the worked problem in various in–class, project, or
homework settings. In this model the Instructor defines the
parametrization in the Offline stage; the Student then specifies
the *parameter values* — within a prescribed (typically very
broad) parameter domain — in the Online stage. (Of course, the
Instructor responsibilities may be assumed by more advanced
Students.) Libraries of worked problems can also be created:
our own library, currently heavily weighted towards heat transfer
— with many steady and unsteady conduction and forced
convection (prescribed velocity) examples — can be found at
`http://augustine.mit.edu/workedProblems.htm`;
for each worked problem we also include a pedagogical guide.

In this paper we first describe the certified reduced ba-
sis method. We then introduce the rbMIT©software package
[6]. Finally, we present results for two illustrative heat transfer
worked problems: a steady thermal fin; and unsteady thermal
analysis of a delamination crack.

2 METHODOLOGY

The methodology in this section is intended for steady and
unsteady heat conduction problems. For the sake of simplicity,
we consider only symmetric spatial operators (conduction) and
compliant outputs. We refer the reader to [19] and references
therein for the treatment of nonsymmetric operators (convection-
diffusion) and general non–compliant outputs. Natural convec-
tion problems can also be treated [3, 10, 22].

2.1 Steady Heat Conduction Problems

Problem Formulation We consider the evaluation of an
output of interest $s_o(\boldsymbol{\mu})$: Given $\boldsymbol{\mu} \in \mathcal{D} \subset \mathbb{R}^P$, we evaluate the

---

output as

$$s_o(\boldsymbol{\mu}) = \int_{B_{oL}} u_o(\boldsymbol{\mu}), \qquad (1)$$

where B_{oL} is part of the domain or domain boundary. Here the
temperature field $u_o(\boldsymbol{\mu})$ satisfies

$$-\frac{\partial}{\partial x_{oi}}\left(\kappa_{oij}^k \frac{\partial u_o(\boldsymbol{\mu})}{\partial x_{oj}}\right) + r_o^k u = f_o^k \text{ in } \Omega_o(\boldsymbol{\mu}), \qquad (2)$$

where $\boldsymbol{\mu}$ is the P-tuple input parameter, $x_o = (x_{o1}, x_{o2})$ denotes a
point in $\Omega_o(\boldsymbol{\mu})$, and $\bar{\Omega}_o(\boldsymbol{\mu}) \equiv \bigcup_{k=1}^{K_{\text{reg}}} \bar{\Omega}_o^k(\boldsymbol{\mu})$ for $\Omega_o^k(\boldsymbol{\mu})$, $1 \leq k \leq K_{\text{reg}}$,
mutually non-overlapping open subdomains of $\Omega_o(\boldsymbol{\mu})$. Also, κ_{oij}^k
is a 2×2 SPD tensor diffusivity, r_o^k is a non–negative scalar, and
f_o^k is a scalar. The boundary conditions are Dirichlet $u_o = u_{oD}$
on Γ_{oD}; general Neumman $n_{oi}\kappa_{oij}^k \frac{\partial u_o(\boldsymbol{\mu})}{\partial x_{oj}} + g_{o1}(u_o(\boldsymbol{\mu}) - g_{o2}) =$
g_{o3} on Γ_{oN}, where $\mathbf{n}_o$ is the outward unit normal, g_{o1} is the Robin
coefficient, g_{o2} is the "sink" field value, and g_{o3} is the flux; and
continuity of temperature and flux at boundaries of $\Omega_o^k(\boldsymbol{\mu})$ which
are internal edges of $\Omega_o(\boldsymbol{\mu})$. Note that all the quantities κ_{oij}^k, r_o^k,
f_o^k, $u_{oD}, g_{o1}, g_{o2}, g_{o3}$ can be *polynomial* functions of x_o and may
also depend on $\boldsymbol{\mu}$.

We now assume a polygonal domain $\Omega_o(\boldsymbol{\mu})$ (though in fact,
with proper care [19], curved domains can also be readily consid-
ered). The RB approach is based on similarity, and we must thus
formulate our parameter–dependent problem on a parameter–
independent reference domain. Towards that end, we construct a
"coarse" triangulation of $\Omega_o(\boldsymbol{\mu})$ that respects all boundaries of all
regions $\Omega_o^k(\boldsymbol{\mu})$, $1 \leq k \leq K_{\text{reg}}$; we then construct a piecewise-affine
mapping which maps the $\boldsymbol{\mu}$-dependent $\bar{\Omega}_o(\boldsymbol{\mu}) \equiv \bigcup_{k=1}^{K_{\text{reg}}} \bar{\Omega}_o^k(\boldsymbol{\mu})$ to a
reference $\boldsymbol{\mu}$-independent $\bar{\Omega} \equiv \bar{\Omega}(\boldsymbol{\mu}_{\text{ref}}) \equiv \bigcup_{k=1}^{K_{\text{reg}}} \bar{\Omega}^k$, where $\boldsymbol{\mu}_{\text{ref}} \in$
$\mathcal{D}$. We can then readily recast [19] our problem for $u_o(\boldsymbol{\mu})$ over
$\Omega_o(\boldsymbol{\mu})$ of (1)–(2) instead as a problem for $u(\boldsymbol{\mu})$ over Ω — (1) and
(2) with all subscript o removed — in which the geometric vari-
ations are now captured by the coefficients of the equation; we
shall henceforth denote this new system of equations by (1)'-(2)'.

In practice, we discretize the problem (2)' by the finite el-
ement (FE) method: Given $\boldsymbol{\mu} \in \mathcal{D} \subset \mathbb{R}^P$, we evaluate $s^{\mathcal{N}}(\boldsymbol{\mu}) =$
$\{\mathbf{L}^{\mathcal{N}}(\boldsymbol{\mu})\}^T\{\mathbf{u}^{\mathcal{N}}(\boldsymbol{\mu})\}$, where the FE temperature solution vector
$\{\mathbf{u}^{\mathcal{N}}\}$ of size $\mathcal{N}$ (which represents the function $u_o^{\mathcal{N}}(\boldsymbol{\mu})$ via the
usual FE basis functions) satisfies $[\mathbf{K}^{\mathcal{N}}(\boldsymbol{\mu})]\{\mathbf{u}^{\mathcal{N}}(\boldsymbol{\mu})\} = \{\mathbf{F}^{\mathcal{N}}(\boldsymbol{\mu})\}$.
Here $[\mathbf{K}^{\mathcal{N}}(\boldsymbol{\mu})]$, $\{\mathbf{L}^{\mathcal{N}}(\boldsymbol{\mu})\}$ and $\{\mathbf{F}^{\mathcal{N}}(\boldsymbol{\mu})\}$ are the FE stiffness
matrix of size $\mathcal{N} \times \mathcal{N}$ and force vector and output vector of
size $\mathcal{N}$, respectively. For simplicity of exposition we assume
that $[\mathbf{K}^{\mathcal{N}}(\boldsymbol{\mu})]$ is symmetric positive-definite, and $\{\mathbf{L}^{\mathcal{N}}(\boldsymbol{\mu})\} =$
$\{\mathbf{F}^{\mathcal{N}}(\boldsymbol{\mu})\}$, so that our model problem is "compliant." We also as-
sume that $\{\mathbf{F}^{\mathcal{N}}(\boldsymbol{\mu})\} \equiv \{\mathbf{F}^{\mathcal{N}}\}$, or $\{\mathbf{F}^{\mathcal{N}}(\boldsymbol{\mu})\}$ is $\boldsymbol{\mu}$-independent; the

extension to the case $\{\mathbf{F}^{\mathcal{N}}(\boldsymbol{\mu})\}$ is $\boldsymbol{\mu}$-dependent is very straightforward [19]. We further assume that the dimension of the FE approximation $\mathcal{N}$ is sufficiently large so that the FE output $s^{\mathcal{N}}(\boldsymbol{\mu})$ is indistinguishable from the exact output $s(\boldsymbol{\mu})$ at the accuracy level of interest.

Finally, we assume that the matrix $[\mathbf{K}^{\mathcal{N}}(\boldsymbol{\mu})]$ is "affine" in the parameter $\boldsymbol{\mu}$, by which we mean

$$[\mathbf{K}^{\mathcal{N}}(\boldsymbol{\mu})] = \sum_{q=1}^{Q} \Theta_q(\boldsymbol{\mu})[\mathbf{K}_q^{\mathcal{N}}]. \qquad (3)$$

Here, for $q = 1, \ldots, Q$, the $\Theta_q : \mathcal{D} \to \mathbb{R}$ are (typically very smooth) $\boldsymbol{\mu}$-dependent functions, and the $[\mathbf{K}_q^{\mathcal{N}}]$ are $\boldsymbol{\mu}$-independent matrices. The affine-parameter decomposition (3) is crucial to the computational performance of the Offline-Online procedure. This assumption is satisfied under rather general hypotheses [19].

Reduced Basis Approximation To define the RB approximation we first introduce our (nested) Lagrangian parameter samples $S_N = \{\boldsymbol{\mu}^1, \ldots, \boldsymbol{\mu}^N\}, 1 \le N \le N_{\max}$, and associated (hierarchical) reduced basis spaces $W_N^{\mathcal{N}}, 1 \le N \le N_{\max}$ [12], $W_N^{\mathcal{N}} = \mathrm{span}\{u^{\mathcal{N}}(\boldsymbol{\mu}^n), 1 \le n \le N\} = \mathrm{span}\{\zeta_n^{\mathcal{N}}, 1 \le n \le N\}$, where $\boldsymbol{\mu}^n \in \mathcal{D}, 1 \le n \le N_{\max}$, are determined by the Greedy sampling method [19]. Note the $\zeta_n^{\mathcal{N}}$ are computed from the snapshots $u^{\mathcal{N}}(\boldsymbol{\mu}^n)$ by a Gram-Schmidt process such that $\{\zeta_m^{\mathcal{N}}\}^T[\mathbf{Y}^{\mathcal{N}}]\{\zeta_n^{\mathcal{N}}\} = \delta_{nm}$, $1 \le m, n \le N$; here δ_{nm} is the Kronecker-delta symbol and $[\mathbf{Y}^{\mathcal{N}}] = [\mathbf{K}^{\mathcal{N}}(\bar{\boldsymbol{\mu}})]$ for some $\bar{\boldsymbol{\mu}} \in \mathcal{D}$.

We then apply a Galerkin projection [1, 8, 11, 19]: given $\boldsymbol{\mu} \in \mathcal{D}$, we evaluate the RB output as $s_N(\boldsymbol{\mu}) = \{\mathbf{F}_N\}^T\{\mathbf{u}_N(\boldsymbol{\mu})\}$, where the RB coefficient N–vector $\{\mathbf{u}_N(\boldsymbol{\mu})\}$ satisfies

$$[\mathbf{K}_N(\boldsymbol{\mu})]\{\mathbf{u}_N(\boldsymbol{\mu})\} = \{\mathbf{F}_N\}. \qquad (4)$$

Here $[\mathbf{K}_N(\boldsymbol{\mu})] = [\mathbf{Z}_N]^T[\mathbf{K}^{\mathcal{N}}(\boldsymbol{\mu})][\mathbf{Z}_N]$ and $\{\mathbf{F}_N\} = [\mathbf{Z}_N]^T\{\mathbf{F}^{\mathcal{N}}\}$ are of dimension $N \times N$ and $N \times 1$, respectively, where $[\mathbf{Z}_N] \equiv [\mathbf{Z}_N^{\mathcal{N}}] = [\{\zeta_1^{\mathcal{N}}\}|\cdots|\{\zeta_N^{\mathcal{N}}\}]$ is the orthonormalized–snapshot matrix of dimension $\mathcal{N} \times N$. We then invoke the affine form (3) to rewrite (4) as $\sum_{q=1}^{Q}\Theta_q(\boldsymbol{\mu})[\mathbf{K}_{qN}]\{\mathbf{u}_N(\boldsymbol{\mu})\} = \{\mathbf{F}_N\}$, where the $[\mathbf{K}_{qN}] = [\mathbf{Z}_N]^T[\mathbf{K}_q^{\mathcal{N}}][\mathbf{Z}_N]$ are parameter-independent matrices of dimension $N \times N$. The Offline-Online strategy is clear.

In the Offline stage, we first compute the $\{\mathbf{u}^{\mathcal{N}}(\boldsymbol{\mu}^n)\}, 1 \le n \le N_{\max}$, form the matrix $[\mathbf{Z}_{N_{\max}}]$ and then form and store $\{\mathbf{F}_{N_{\max}}\}$ and $[\mathbf{K}_{qN_{\max}}]$. The Offline operation count depends on $N_{\max}, Q$ and $\mathcal{N}$ but requires only $O(QN_{\max}^2)$ permanent storage. In the Online stage, for a given $\boldsymbol{\mu}$ and N $(1 \le N \le N_{\max})$, we retrieve the pre-computed $[\mathbf{K}_{qN}]$ and $\{\mathbf{F}_N\}$ (subarrays of $[\mathbf{K}_{qN_{\max}}], \{\mathbf{F}_{N_{\max}}\}$), form $[\mathbf{K}_N(\boldsymbol{\mu})]$, solve the resulting $N \times N$ system (4) to obtain

$\{\mathbf{u}_N(\boldsymbol{\mu})\}$, and finally evaluate the output s_N. The Online operation count is thus $O(N^3)$ and independent of $\mathcal{N}$. The implication of the latter is two-fold: first, we will achieve very fast response in the many-query and real-time contexts, as N is typically very small, $N \ll \mathcal{N}$; and second, we can choose $\mathcal{N}$ arbitrary large – to obtain as accurate FE predictions as we wish – without adversely affecting the Online (marginal) cost.

Reduced Basis Error Estimator We now define our error estimator and associated effectivity for the output as $\Delta_N^s(\boldsymbol{\mu}) = \varepsilon^2(\boldsymbol{\mu})/\alpha_{\mathrm{LB}}^{\mathcal{N}}(\boldsymbol{\mu})$ and $\eta_N^s(\boldsymbol{\mu}) = \Delta_N^s(\boldsymbol{\mu})/(s^{\mathcal{N}}(\boldsymbol{\mu}) - s_N(\boldsymbol{\mu}))$, where $\varepsilon^2(\boldsymbol{\mu}) = \{\mathbf{R}^{\mathcal{N}}\}^T[\mathbf{Y}^{\mathcal{N}}]^{-1}\{\mathbf{R}^{\mathcal{N}}\}$ is the square of the dual norm of the residual vector $\{\mathbf{R}^{\mathcal{N}}\} = \{\mathbf{F}^{\mathcal{N}}\} - [\mathbf{K}^{\mathcal{N}}(\boldsymbol{\mu})][\mathbf{Z}_N]\{\mathbf{u}_N(\boldsymbol{\mu})\}$, and $\alpha_{\mathrm{LB}}^{\mathcal{N}}(\boldsymbol{\mu})$ is a lower bound for the discrete coercivity constant [19][2]. The effectivity $\eta_N^s(\boldsymbol{\mu})$ is a measure of the quality of the proposed estimator; we can show that $\eta_N^s(\boldsymbol{\mu}) \ge 1$, and hence our error estimator is a rigorous upper bound.

The calculation of the dual norm of the residual is rather simple. Following the procedure described in [19], $\varepsilon^2(\boldsymbol{\mu})$ can be expressed as

$$\varepsilon^2(\boldsymbol{\mu}) = \underbrace{\{\mathbf{C}\}^T[\mathbf{Y}^{\mathcal{N}}]\{\mathbf{C}\}}_{1 \times 1} + 2\sum_{q=1}^{Q}\Theta_q(\boldsymbol{\mu})\{\mathbf{u}_N(\boldsymbol{\mu})\}^T\underbrace{[\mathbf{B}_q]^T[\mathbf{Y}^{\mathcal{N}}]\{\mathbf{C}\}}_{N \times 1}$$
$$+ \sum_{q=1}^{Q}\sum_{q'=1}^{Q}\Theta_q(\boldsymbol{\mu})\Theta_{q'}(\boldsymbol{\mu})\{\mathbf{u}_N(\boldsymbol{\mu})\}^T\underbrace{[\mathbf{B}_{q'}]^T[\mathbf{Y}^{\mathcal{N}}][\mathbf{B}_q]}_{N \times N}\{\mathbf{u}_N(\boldsymbol{\mu})\}, \quad (5)$$

where $\{\mathbf{C}\} = [\mathbf{Y}^{\mathcal{N}}]^{-1}\{\mathbf{F}^{\mathcal{N}}\}$ and $[\mathbf{B}_q] = -[\mathbf{Y}^{\mathcal{N}}]^{-1}[\mathbf{K}_q^{\mathcal{N}}][\mathbf{Z}_N]$ are quantities formed from FE solutions.

The computation of $\varepsilon^2(\boldsymbol{\mu})$ readily admits an Offline-Online strategy: all the underbraced matrix-matrix or matrix-vector products are $\boldsymbol{\mu}$-independent and can be pre-computed in the Offline stage – with $O(Q^2N_{\max}^2)$ permanent storage; the computational cost in the Online stage is then $O(Q^2N_{\max}^2)$ – independent of $\mathcal{N}$. The low marginal cost of the error estimator also plays a crucial role in our greedy construction of the optimal RB parameter sample set $S_{N_{\max}}$ [19].

2.2 Unsteady Heat Conduction Problems
Problem Formulation We now consider the unsteady version of the above model problem (which we state directly for the reference domain): Given $\boldsymbol{\mu} \in \mathcal{D} \subset \mathbb{R}^P$, we evaluate the out-

---

[2]The discrete coercivity constant is, in essence, a generalized minimum eigenvalue; we invoke the SCM method [19], [5] to calculate $\alpha_{\mathrm{LB}}^{\mathcal{N}}(\boldsymbol{\mu})$. The Online evaluation of $\alpha_{\mathrm{LB}}^{\mathcal{N}}(\boldsymbol{\mu})$ does not depend on $\mathcal{N}$ and hence we can retain rapid response in the many-query and real-time contexts.

put[3] as

$$s(\boldsymbol{\mu}) = \int_0^{t_f} \left(h(t) \int_{B_L} u(t;\boldsymbol{\mu}) \right) dt, \qquad (6)$$

where the temperature field $u(t;\boldsymbol{\mu})$ is the solution of the time-dependent parametrized PDE

$$\frac{\partial u}{\partial t} - \frac{\partial}{\partial x_i} \left(\kappa_{ij}^k \frac{\partial u}{\partial x_j} \right) + r^k u = g(t) f^k \text{ in } \Omega(\boldsymbol{\mu}), \qquad (7)$$

with initial condition $u(t = 0;\boldsymbol{\mu}) = u_0$. Here $t \in (0,t_f]$ is the time variable, and $h(t) \in L^2((0,t_f])$ and $g(t) \in L^2((0,t_f])$ are the output and input (control) functions of t. We assume the same boundary conditions as before, however, now g_1, g_2, and g_3 may depend on t as well.

We next introduce the semi-discrete FE approximation for (6)-(7): Given $\boldsymbol{\mu} \in \mathcal{D} \subset \mathbb{R}^P$, we evaluate $s^{\mathcal{N}}(\boldsymbol{\mu}) = \int_0^{t_f} \left(h(t)\{\mathbf{L}^{\mathcal{N}}\}^T \{\mathbf{u}^{\mathcal{N}}(t;\boldsymbol{\mu})\} \right) dt$, where the FE temperature vector $\mathbf{u}^{\mathcal{N}}(t;\boldsymbol{\mu})$ of size $\mathcal{N}$ satisfies for $t \in (0,t_f]$

$$[\mathbf{M}^{\mathcal{N}}(\boldsymbol{\mu})]\{\dot{\mathbf{u}}^{\mathcal{N}}(t;\boldsymbol{\mu})\} + [\mathbf{K}^{\mathcal{N}}(\boldsymbol{\mu})]\{\mathbf{u}^{\mathcal{N}}(t;\boldsymbol{\mu})\} = g(t)\{\mathbf{F}^{\mathcal{N}}\}, \quad (8)$$

with initial condition $\mathbf{u}^{\mathcal{N}}(t = 0;\boldsymbol{\mu}) = \mathbf{u}_0^{\mathcal{N}}$. Here $[\mathbf{M}^{\mathcal{N}}(\boldsymbol{\mu})]$ is the FE mass matrix, which we assume is symmetric positive-definite and affine in the parameter $[\mathbf{M}^{\mathcal{N}}(\boldsymbol{\mu})] = \sum_{j=1}^J \Phi_j(\boldsymbol{\mu})[\mathbf{M}_j^{\mathcal{N}}]$, where, for $j = 1,\ldots,J$, the $\Phi_j : \mathcal{D} \to \mathbb{R}$ are $\boldsymbol{\mu}$-dependent functions and the $[\mathbf{M}_j^{\mathcal{N}}]$ are $\boldsymbol{\mu}$-independent matrices.

In actual practice we apply the Euler-Backward scheme for the temporal discretization of the system (8) and the trapezoidal rule for the integral (6). For brevity in this paper we shall describe the RB methodology only for the semi–discrete formulation (8), however all of our results — including the rigorous error estimator — extend to fully discrete case that we actually consider in practice [4, 8].

Reduced Basis Approximation We begin by introducing the hierarchical RB spaces $W_N^{\mathcal{N}} = \text{span}\{\zeta_n^{\mathcal{N}}, 1 \le n \le N\}, 1 \le N \le N_{\max}$; the basis functions $\zeta_n^{\mathcal{N}}, 1 \le n \le N_{\max}$, are determined by a POD-Greedy sampling method [8, 9]. As before, $[\mathbf{Z}_N] \equiv [\mathbf{Z}_N^{\mathcal{N}}] = [\{\boldsymbol{\zeta}_1^{\mathcal{N}}\}|\cdots|\{\boldsymbol{\zeta}_N^{\mathcal{N}}\}]$ is the snapshot matrix of dimension $\mathcal{N} \times N$.

We now apply Galerkin projection: given $\boldsymbol{\mu} \in \mathcal{D}$, we evaluate the RB output as $s_N(\boldsymbol{\mu}) = \int_0^{t_f} \left(h(t)\{\mathbf{L}_N\}^T \{\mathbf{u}_N(t;\boldsymbol{\mu})\} \right) dt$,

where $\{\mathbf{u}_N(t;\boldsymbol{\mu})\}$ satisfies the evolution equation $\sum_{j=1}^J \Phi_j(\boldsymbol{\mu})[\mathbf{M}_{jN}]\{\dot{\mathbf{u}}_N(t;\boldsymbol{\mu})\} + \sum_{q=1}^Q \Theta_q(\boldsymbol{\mu})[\mathbf{K}_{qN}]\{\mathbf{u}_N(t;\boldsymbol{\mu})\} = g(t)\{\mathbf{F}_N\}$. We have directly exploited our affine representations for stiffness and mass matrices: $\{\mathbf{L}_N\} = [\mathbf{Z}_N]^T\{\mathbf{L}^{\mathcal{N}}\}$, $\{\mathbf{F}_N\} = [\mathbf{Z}_N]^T\{\mathbf{F}^{\mathcal{N}}\}$, $[\mathbf{K}_{qN}] = [\mathbf{Z}_N]^T[\mathbf{K}_q^{\mathcal{N}}][\mathbf{Z}_N], 1 \le q \le Q$, and $[\mathbf{M}_{jN}] = [\mathbf{Z}_N]^T[\mathbf{M}_j^{\mathcal{N}}][\mathbf{Z}_N], 1 \le j \le J$.

The Offline-Online procedure is now straightforward; in particular, the unsteady case is very similar to the steady case discussed in detail in the previous section. There are a few new twists: as regards storage, we must now append to the elliptic Offline dataset an affine development for the mass matrix $[\mathbf{M}_{jN}], 1 \le j \le J$, associated with the unsteady term; as regards computational complexity, we must multiply the elliptic operation counts by K to arrive at $O(KN^3)$ (in fact, $O(KN^2)$ for a Linear-Time-Invariant system) for the Online operation count, where K is the number of time steps in our temporal discretization. (Recall that in actual practice our "truth" is discrete in time.) Thus, the Online evaluation of $s_N(\boldsymbol{\mu})$ remains independent of $\mathcal{N}$ even in the unsteady case.

Reduced Basis Error Estimator We can now define the *a posteriori* error estimator for $|s^{\mathcal{N}}(\boldsymbol{\mu}) - s_N(\boldsymbol{\mu})|$ as $\Delta_N^s(\boldsymbol{\mu}) = \frac{\sigma_0}{\alpha_{\text{LB}}^{\mathcal{N}}(\boldsymbol{\mu})} \left(\left(\int_0^{t_f} h^2(t) dt \right) \left(\int_0^{t_f} \varepsilon^2(t;\boldsymbol{\mu}) dt \right) \right)^{1/2}$, where $\sigma_0^2 = \{\mathbf{L}^{\mathcal{N}}\}^T[\mathbf{Y}^{\mathcal{N}}]^{-1}\{\mathbf{L}^{\mathcal{N}}\}$ is the square of the dual norm of the output vector $\mathbf{L}^{\mathcal{N}}$ and $\varepsilon^2(t;\boldsymbol{\mu}) = \{\mathbf{R}^{\mathcal{N}}\}^T[\mathbf{Y}^{\mathcal{N}}]^{-1}\{\mathbf{R}^{\mathcal{N}}\}$ is the square of the dual norm of the residual vector $\{\mathbf{R}^{\mathcal{N}}(t;\boldsymbol{\mu})\} = g(t)\{\mathbf{F}^{\mathcal{N}}\} - \sum_{j=1}^J \Phi_j(\boldsymbol{\mu})[\mathbf{M}_j^{\mathcal{N}}][\mathbf{Z}_N]\{\dot{\mathbf{u}}_N(t;\boldsymbol{\mu})\} - \sum_{q=1}^Q \Theta_q(\boldsymbol{\mu})[\mathbf{K}_q^{\mathcal{N}}][\mathbf{Z}_N]\{\mathbf{u}_N(t;\boldsymbol{\mu})\}$. Of course, in practice, we apply the trapezoidal rule for the integral in the error bound and the Euler-Backward scheme for the residual expression. Then both $\Delta_N^s(\boldsymbol{\mu})$ and $\varepsilon^2(t;\boldsymbol{\mu})$ can be expressed as sums of products of $\boldsymbol{\mu}$-dependent coefficients and $\boldsymbol{\mu}$-independent quantities as shown in the steady case.

Therefore, we can readily adapt the Offline-Online strategy developed in the steady case to the unsteady case — with the few twists already described in the previous subsection. The crucial point, again, is that the cost and storage in the Online stage — the *marginal* cost to evaluate $\Delta_N^s(\boldsymbol{\mu})$ for each new value of $\boldsymbol{\mu}$ — is independent of $\mathcal{N}$: thus we can not only evaluate our output prediction but also our rigorous output error bound very rapidly in the parametrically interesting contexts of real-time or many-query investigation. In short, we inherit the high fidelity and certainty of the FE approximation but at the low cost of a reduced-order model.

Finally, it should be noted that both the RB output and associated error bound are rather crude. In actual practice, in particular in the rbMIT© software, we pursue primal-dual reduced basis approximations that provide both more rapid convergence of the RB output and also more robust (sharper) estimation of

---

[3]It is also possible for certain output functionals to (efficiently) evaluate $s(t;\boldsymbol{\mu})$ for all $t \in (0,t_f]$ [8].

the output error. The primal-dual RB approach requires the introduction of an adjoint problem, which admits a very similar RB treatment as the primal problem (8) described here. We refer the reader to [4] for details of the primal-dual RB approach.

3 THE rbMIT©MIT SOFTWARE

The rbMIT© software package implements in Matlab® all the general RB algorithms, [6]. The rbMIT© Software architecture can be divided into three steps: the Problem Formulation Step, the RB Offline Step, and the RB Online Step.

The User Input   The user must describe the problem. The input can be separated into three parts: the geometry, the "material," and the parameter control. For geometry input, the user must describe the geometry $\Omega_o(\boldsymbol{\mu})$ by providing points coordinates (which can be a function of $\boldsymbol{\mu}$), straight or curvy edges that describe all regions (or holes), and finally the regions $\Omega_o^k(\boldsymbol{\mu})$ in terms of the provided edges. For material input, the user must provide the necessary coefficients in Eqn. (2) for each region $\Omega_o^k(\boldsymbol{\mu})$ as well as the coefficients in the boundary conditions. For parameter control, the user must provide the parameter domain $\mathcal{D}$, or a functional that describes the "in-out" properties of a point $\boldsymbol{\mu} \in \mathbb{R}^P$ with respect to $\mathcal{D}$ (and also reference parameters for the reference mapping and inner product). The user should also provide information which describes stopping criteria for the RB sample set construction, for example $N_{\max}$ or the RB error tolerance. The user inputs are provided in a relatively simple "rbU" file; examples may be found in the rbMIT documentation at http://augustine.mit.edu/methodology/.. ../methodology_rbMIT_System.htm.

The Problem Formulation Step   This step constructs the underlying "truth" FE discretization in an affine representation suitable for subsequent Offline-Online RB approximation. First, our coarse triangulation is constructed using data provided in the User Input and a custom constrained Delaunay triangulation algorithm with special considerations for curvy edges. Geometric transformations are then constructed symbolically for each sub-triangle, which — coupled to the material input — generate variable ($\boldsymbol{\mu}$-dependent) coefficients $\Theta_q(\boldsymbol{\mu})$ for each sub-triangle. In actual practice, the $\Theta_q(\boldsymbol{\mu})$ functions are then combined, by eliminating duplicated or proportional terms, to minimize Q. At the final stage, a FE mesh — which conforms to all edges of all sub-triangles — is generated and discrete FE stiffness matrices and vectors are assembled for each sub-triangle (and then combined) to form the $\boldsymbol{\mu}$-independent components of Eqn. (3). Note that all ($\boldsymbol{\mu}$-dependent) $\Theta_q(\boldsymbol{\mu})$ functions are stored as symbolic quantities while all ($\boldsymbol{\mu}$-independent) FE matrices and vectors component are stored as numeric quantities[4].

The RB Offline Step   This step first generates the Offline data for the computation of the lower bound of the coercivity constant [5]. Next, a greedy algorithm is invoked to obtain the RB parameter sample set $S_{N_{\max}}$ and $[\mathbf{Z}_{N_{\max}}]$. Finally, $\{\mathbf{F}_{N_{\max}}\}$, $[\mathbf{K}_{qN_{\max}}]$, and all underbraced quantities in (5) are then saved in an "Online Database" (of size $O(Q^2 N_{\max}^2)$) for use by the RB Online Step. The RB Offline step is the most computationally expensive step since the operation count depends on $\mathcal{N}$.

The RB Online Step   In this stage, given an input parameter value in the parameter domain, the RB Online Evaluator retrieves the minimal pre-computed data from the "Online Database" and returns both (a) an accurate RB prediction for the output, $s_N(\boldsymbol{\mu})$, and (b) a certificate of fidelity that rigorously bounds the error in the RB prediction relative to the highly accurate truth finite element solution, $\Delta_N^s(\boldsymbol{\mu})$. For example, for the (steady) problem named probname = 'fin' with output named outputname = 'average', the Matlab syntax to calculate the RB output (sN) and the associated error estimation (DeltaN) for $\boldsymbol{\mu} = [0.1, 3, 1]$ is [sN, DeltaN] = Online RB('fin',[.1,3,1],'average')[5]. The operation count for the RB Online step is very low, independent of the resolution of the FE approximation.

The RB Visualizer (a) renders the relevant field variable, and (b) provides an associated rigorous bound for the error in the RB field relative to the finite element field. In RB Visualizer, the computational cost to recreate the RB field depends on $\mathcal{N}$ — $O(N\mathcal{N})$ — however for small N real-time response can still be attained.

4 ILLUSTRATIVE WORKED PROBLEMS

In this section we describe the application of the RB methodology to two examples ("worked problems") dealing with steady and unsteady heat transfer: (1) a thermal fin problem, and (2) a nonhomogeneous semi-infinite body problem [20]. These problems (and many others) are available at the address http://augustine.mit.edu/workedProblems.htm for download or via a Matlab ® webserver.

––––––––

[4]The current rbMIT© software supports several PDE engines for the generation of the FE mesh and all FE matrices and vectors, including the Matlab®PDEtoolbox, the commercial software COMSOL®, and a "home–brew" PDE engine.

[5]This Matlab command-line entry illustrates both the simple inputs required on the part of the Student as well as the "constrained flexibility" allowed the Student: although the values of the three inputs are specified by the Student (Online), the definition of these input parameters (described in Section 4.1) and the domain $\mathcal{D}$ over which these parameters can vary is prescribed by the Instructor.

4.1 The Thermal Fin Problem

This problem considers the performance of a heat sink designed for the thermal management of high-density electronic components. The heat sink, shown in Fig. 1, comprises a base/spreader which in turn supports a number of plate fins exposed to flowing air; we shall consider the shaded domain — one half of one fin in the multi-fin sink — due to assumed periodicity and symmetry. We model the flowing air through a simple convection heat transfer coefficient; our interest is in the temperature at the base of the spreader. From the engineering point of view, this problem illustrates the application of conduction analysis [2] to an important class of cooling problems: electronic components and systems. From the physical point of view, this
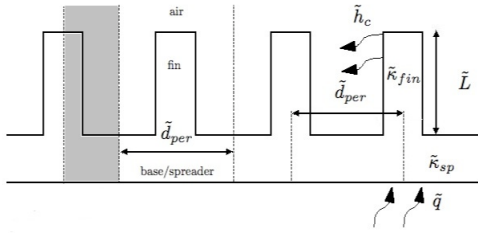

Figure 1. Heat sink problem.

worked problem illustrates many aspects of steady conduction heat transfer: (*i*) the basic elements of thermal resistance, (*ii*) the notion of a constriction resistance, and most importantly (*iii*) the utility of the "thermal fin" concept, and (*iv*) the relevance of the classical "1-D thermal fin" idealization.

We assume that the spreader has thermal conductivity $\tilde{\kappa}_{sp}$ and that the plate fin has thermal conductivity $\tilde{\kappa}_{fin}$; we denote the ratio of these conductivities as $\kappa \equiv \tilde{\kappa}_{sp}/\tilde{\kappa}_{fin}$. The distance between neighboring fins (and by assumption twice the thickness of the fins) is denoted $\tilde{d}_{per}$, while the height of the fin is denoted $\tilde{L}$. We characterize the heat transfer from the fin to the air by a heat transfer coefficient $\tilde{h}_c$ and the corresponding non-dimensional Biot number, $\mathrm{Bi} \equiv \tilde{h}_c \tilde{d}_{per}/\tilde{\kappa}_{fin}$. Note that a tilde ˜ denotes dimensional quantities, and the absence of a tilde signals a non-dimensional quantity. We shall consider here $P = 3$ parameters. Here μ_1 is the Biot number, Bi, $\mu_2 \equiv L = \tilde{L}/\tilde{d}_{per}$, the nondimensional fin height, and μ_3 is the spreader-to-fin conductivity ratio, κ. The parameter domain is given by $\mathcal{D} = [0.01, 0.5] \times [2, 8] \times [1, 10]$.

The temperature is measured relative to the temperature of the air "at infinity" and non-dimensionalized with respect to $(\tilde{q}\tilde{d}_{per}/\tilde{\kappa}_{fin})$, where $\tilde{q}$ is the dimensional heat flux into the spreader base; the spatial coordinate $\tilde{x} = (\tilde{x}_{o1}, \tilde{x}_{o2})$ is nondimensionalized with respect to $\tilde{d}_{per}$. We identify in Fig. 2 the points and regions $\Omega_o^k(\boldsymbol{\mu})$, $1 \le k \le 2$, which will serve to define the nondimensional geometry and physical properties.
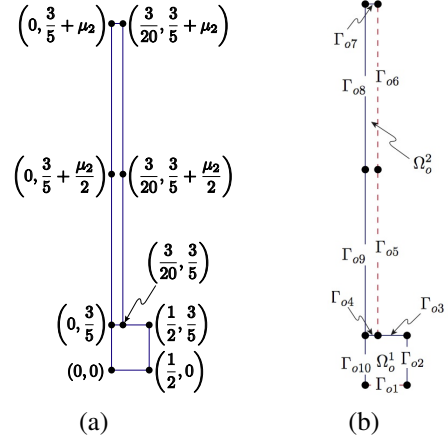

Figure 2. Heat sink: parametrized geometry and boundary.

The steady-state (non-dimensional) temperature distribution $u_o(\boldsymbol{\mu})$ over the (non-dimensional) domain $\Omega_o(\boldsymbol{\mu})$ satisfies the conduction equation. We impose continuity of temperature and heat flux at the spreader-fin interface; zero heat flux (conservatively) on the horizontal exposed surfaces of the spreader and fin; uniform heat flux at the base of the spreader (as a model of the Joule heating from the electronic component); heat-transfer coefficient/convection (Robin) boundary conditions on the vertical face of the fin — the surface exposed to the flowing air; and a symmetry condition on the other vertical cuts.

Mathematically, $u_o(\boldsymbol{\mu})$ satisfies

$$-\frac{\partial}{\partial x_{oi}}\left(\underbrace{\begin{bmatrix} \mu_3 & 0 \\ 0 & \mu_3 \end{bmatrix}}_{\kappa_{oij}^1}\frac{\partial}{\partial x_{oj}}u_o(\boldsymbol{\mu})\right) = 0 \text{ in } \Omega_o^1, \qquad (9)$$

$$-\frac{\partial}{\partial x_{oi}}\left(\underbrace{\begin{bmatrix} 1 & 0 \\ 0 & 1 \end{bmatrix}}_{\kappa_{oij}^2}\frac{\partial}{\partial x_{oj}}u_o(\boldsymbol{\mu})\right) = 0 \text{ in } \Omega_o^2(\mu_2), \qquad (10)$$

with summation $(i, j = 1, 2)$ over repeated indices. On the internal interface Γ_{o4} (between the two regions), we impose continuity of temperature $u_o(\boldsymbol{\mu})$ and heat flux $\mathbf{n}_{oi}\kappa_{oij}\frac{\partial}{\partial x_{oj}}u_o(\boldsymbol{\mu})$, where $\mathbf{n}_{oi}$ denotes unit outward normal. On boundaries Γ_{o2}, Γ_{o3}, Γ_{o7}, Γ_{o8}, Γ_{o9} and Γ_{o10} we impose homogeneous Neumann conditions, $\mathbf{n}_{oi}\kappa_{oij}\frac{\partial}{\partial x_{oj}}u_o(\boldsymbol{\mu}) = 0$. Finally we impose a non-homogeneous Neumann condition, $\mathbf{n}_{oi}\kappa_{oij}^1\frac{\partial u_o}{\partial x_{oj}}(\boldsymbol{\mu}) = 1$ on Γ_{o1}, and the Robin conditions, $\mathbf{n}_{oi}\kappa_{oij}^2\frac{\partial u_o}{\partial x_{oj}}(\boldsymbol{\mu}) + (\mu_1)u_o = 0$ on Γ_{o5}, $\mathbf{n}_{oi}\kappa_{oij}^2\frac{\partial u_o}{\partial x_{oj}}(\boldsymbol{\mu}) + (\mu_1)u_o = 0$ on Γ_{o6}, corresponding to flux and heat-transfer coefficient/convection, respectively.

7

The output for this problem is the average temperature over the base of the spreader — which corresponds not only to the point of interest (the electronic component to be cooled) but also to the hottest location in the system. We denote this output by $T_{o\,av}(\boldsymbol{\mu}) = 2\int_{\Gamma_{o1}} u_o(\boldsymbol{\mu})$; note the output will depend on our three parameters, $\mu \equiv (\mathrm{Bi}, L, \kappa)$. (Recall that this output is nondimensionalized: to translate $T_{o\,av}(\mu)$ into a dimensional temperature we must multiply by $\tilde{q}\tilde{d}_{\mathrm{per}}/\tilde{\kappa}_{\mathrm{fin}}$ and then add the ambient temperature level.) Other outputs of interest may include the average temperature at the root of the fin (i.e., at the spreader-fin interface), and the average temperature at the tip of the fin (related to fin efficiency).

This problem is then mapped to our fixed reference domain Ω and subsequently discretized by a P_1 finite element (FE) discretization [14]; the FE space contains $\mathcal{N} = 4198$ degrees of freedom. This FE approximation is typically too slow for many applications, and we hence approximate the FE prediction for the output and field variable by the certified reduced basis method described in the previous section.

We present in Figure 3 our results as a plot of the RB output and RB error bars — defined as the interval $[s_N(\boldsymbol{\mu}) - \Delta_N^s(\boldsymbol{\mu}), s_N(\boldsymbol{\mu}) + \Delta_N^s(\boldsymbol{\mu})]$ in which the truth FE solution *must* reside — as a function of μ_1 for $\mu_2 = 2$ and $\mu_3 = 1$ for $N = 6$. (Here N actually refers to the number of primal modes and dual modes within our primal–dual formulation [13, 19].) These results demonstrate the small value of N required to achieve certified high accuracy; these results also demonstrate the importance of the error bounds not only in certifying the results but also in ensuring efficiency — permitting us to *safely* choose a small value of N without sacrificing accuracy or certainty. The method also converges very quickly — increasing N to 13 reduces the certified error (maximum error bar in Figure 3) by a factor of 10^2— the error bars are no longer discernable.

As regards computational times, a RB Online evaluation requires on average 0.13s for $N = 7$ and 0.15s for $N = 13$, including both $s_N(\boldsymbol{\mu})$ and $\Delta_N^s(\boldsymbol{\mu})$; FEM solution $\boldsymbol{\mu} \to s^{\mathcal{N}}(\boldsymbol{\mu})$ requires 1.96s to be completed. Hence an average Online evaluation requires only $5 - 6\%$ of the FEM computational cost. This fin model is only two-dimensional; of course a three-dimensional model is possible and in this case the RB computational advantages will be even more significant.

4.2 Delamination Crack

This worked problem considers the transient evolution of the temperature field near the surface of a Fiber-Reinforced-Polymer (FRP) Concrete (C) slab [20]. The FRP is affixed or retrofitted to concrete or masonry surfaces to strengthen or rehabilitate the (infra)structure; unfortunately, the FRP is susceptible to delamination, and the formation of cracks at the FRP-Concrete interface can jeopardize integrity [8, 20]. The problem geometry — FRP, C, and delamination crack — is shown in Figure 4 (note that
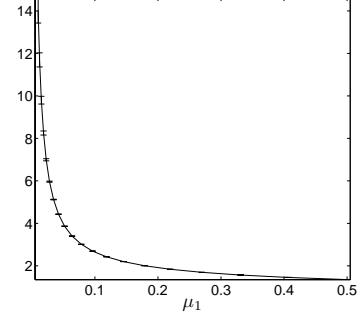

Figure 3. RB output and RB error bars — defined as the interval $[s_N(\boldsymbol{\mu}) - \Delta_N^s(\boldsymbol{\mu}), s_N(\boldsymbol{\mu}) + \Delta_N^s(\boldsymbol{\mu})]$ — as a function of μ_1 for $\mu_2 = 2$, $\mu_3 = 1$ and $N = 6$.

Figure 4 is not drawn to scale in the vertical direction). From the engineering point of view, the inverse version of this problem illustrates the application of transient conduction to real-time nondestructive evaluation — here, crack detection. From the physical point of view, this problem illustrates (*i*) the basic time scales associated with transient conduction, and (*ii*) the dependence of temperature field evolution on material and geometric inhomogeneities.

The key components are the FRP layer above of depth $\tilde{d}_{\mathrm{FRP}}$; the Concrete slab below (effectively of infinite depth); and the delamination crack of length $2\tilde{w}_{\mathrm{del}}$ — modeled as an insulating infinitely thin gap — at the interface between the FRP and the Concrete. The critical physical properties are the density, specific heat, and conductivity which we shall denote by $\tilde{\rho}$, $\tilde{c}$, and $\tilde{\kappa}$ respectively; subscripts FRP and C shall refer to the FRP and the Concrete components, respectively. We shall assume that $\tilde{\rho}_C\tilde{c}_C = \tilde{\rho}_{\mathrm{FRP}}\tilde{c}_{\mathrm{FRP}}$; hence $\kappa = \tilde{\kappa}_{\mathrm{FRP}}/\tilde{\kappa}_C$, the ratio of the FRP and Concrete conductivities, is also the ratio of the FRP and Concrete thermal diffusivities. (We exploit this coincidence/simplification in our formulation.) We consider $P = 3$ parameters. Here μ_1 and μ_2 are geometry parameters: $\mu_1 \equiv \tilde{w}_{\mathrm{del}}/\tilde{d}_{\mathrm{FRP}}^{\max}$ is the nondimensional delamination crack width, and $\mu_2 \equiv \tilde{d}_{\mathrm{FRP}}/\tilde{d}_{\mathrm{FRP}}^{\max}$ is the nondimensional crack location — the thickness of the FRP layer; note $\tilde{d}_{\mathrm{FRP}}^{\max}$ is the maximum FRP layer thickness of interest. The remaining (always non-dimensional) parameter is $\mu_3 = \kappa$, the ratio of the FRP and Concrete thermal conductivities (and coincidentally, diffusivities). The parameter domain is given by $\mathcal{D} = [0.1, 1] \times [0.1, 1] \times [0.4, 1.8]$.

The temperature is measured relative to the initial temperature and non-dimensionalized with respect to $\tilde{q}\tilde{d}_{\mathrm{FRP}}^{\max}/\tilde{\kappa}_{\mathrm{FRP}}$, where $\tilde{q}$ is the dimensional heat flux imposed at the top boundary; the spatial coordinate $(\tilde{x}_{o1}, \tilde{x}_{o2})$ is nondimensionalized with respect to $\tilde{d}_{\mathrm{FRP}}^{\max}$; and the temporal variable $\tilde{t}$ is nondimensionalized with $\tilde{\rho}_{\mathrm{FRP}}\tilde{c}_{\mathrm{FRP}}(\tilde{d}_{\mathrm{FRP}}^{\max})^2/\tilde{\kappa}_{\mathrm{FRP}}$. We identify in Figure 5 the nondimensional points, regions Ω_o^k, $1 \leq k \leq 2$, and boundary/interfaces Γ_o. which will serve to define the geometry and physical properties.
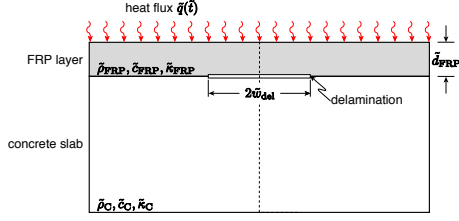
8

Figure 4. Delamination crack in FRP bonded to Concrete.
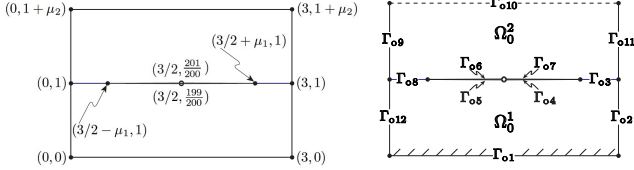

Figure 5. Delamination crack: Parametrized geometry.

The nondimensional temperature $u_o(t, \boldsymbol{\mu})$ over the (nondimensional) domain Ω_o and time interval $[0, t_f = 2.5]$ is governed by the heat (or diffusion) equation. (Note a final time of t_f is sufficient for the surface flux to reach (beyond) the crack.) We impose continuity of temperature and heat flux at the FRP-C interface; zero temperature at the bottom of the C layer; uniform but time–dependent heat flux at the FRP surface; and zero flux conditions on all other boundaries, including the (two) crack surfaces.

Mathematically, $u_o(\boldsymbol{\mu})$ satisfies for $t \in (0, t_f]$

$$\frac{\partial u_o(\boldsymbol{\mu})}{\partial t} - \frac{\partial}{\partial x_{oi}} \left(\underbrace{\begin{bmatrix} 1 & 0 \\ 0 & 1 \end{bmatrix}}_{\kappa^1_{oij}} \frac{\partial}{\partial x_{oj}} u_o(\boldsymbol{\mu}) \right) = 0 \qquad \text{in } \Omega_o^1(\boldsymbol{\mu}),$$

$$\frac{\partial u_o(\boldsymbol{\mu})}{\partial t} - \frac{\partial}{\partial x_{oi}} \left(\underbrace{\begin{bmatrix} \mu_3 & 0 \\ 0 & \mu_3 \end{bmatrix}}_{\kappa^2_{oij}} \frac{\partial}{\partial x_{oj}} u_o(\boldsymbol{\mu}) \right) = 0 \qquad \text{in } \Omega_o^2(\boldsymbol{\mu}),$$

with initial condition $u_o(t = 0) = 0$. On the FRP-C interfaces, we impose continuity of temperature and heat flux $\mathbf{n}_{oi} \kappa_{oij} \frac{\partial}{\partial x_{oj}} u_o(\boldsymbol{\mu})$. On boundary Γ_{o1} (the C bottom) we impose homogeneous Dirichlet conditions $u_o(\boldsymbol{\mu}) = 0$. On boundary Γ_{o10} (the FRP surface) we impose a non-homogeneous Neumann condition, $\mathbf{n}_{oi} \kappa^2_{oij} \frac{\partial u_o(\boldsymbol{\mu})}{\partial x_{oj}} = g(t)$ on Γ_{o10}, where the control input $g(t)$ may be any square-integrable function of time t. Finally, on boundaries Γ_{o2}, Γ_{o4}, Γ_{o5}, Γ_{o6}, Γ_{o7}, Γ_{o9}, Γ_{o11} and Γ_{o12} we impose homogeneous Neumann conditions (insulation),

$$\mathbf{n}_{oi} \kappa_{oij} \frac{\partial}{\partial x_{oj}} u_o(\boldsymbol{\mu}) = 0.$$

The output of interest is the integral of the average temperature of the FRP layer over the time interval $(0, t_f)$: $s(\boldsymbol{\mu}) = \frac{1}{3\mu_2} \int_0^{t_f} \left(h(t) \int_{\Omega_o^2} u_o(t; \boldsymbol{\mu}) \right) dt$, where we recall that the final time is $t_f = 2.5$. Although $h(t)$ can be any square-integrable function of t, we consider here $h(t) = 1$ in our numerical experiments. In actual practice, we consider more interesting outputs [8] — average temperatures over small measurement sites as a function of time — but for simplicity of exposition here we restrict attention only to a simpe output.

This problem is then mapped to our fixed reference domain and subsequently discretized by a P_1 linear FE approximation space of $\mathcal{N} = 1,912$ degrees of freedom in space and the Euler-backward scheme with a constant timestep $\Delta t = 0.05$ in time. The number of time steps is thus $K = 50$ for our final time $t_f = 2.5$. We consider the particular case in which $g(t) = t$ for $t \leq 1.25$ and $g(t) = 2.5 - t$ for $t > 1.25$. Note that $g(t)$ — thanks to "impulse training" RB space — need be specified only in the Online stage [4].

We present our results in a fashion similar to the steady case. We plot in Figure 6 for $N = 25$ the RB output and RB error bars — defined as the interval $[s_N(\boldsymbol{\mu}) - \Delta_N^s(\boldsymbol{\mu}), s_N(\boldsymbol{\mu}) + \Delta_N^s(\boldsymbol{\mu})]$ in which the truth FE output $s^{\mathcal{N}}(\boldsymbol{\mu})$ *must* reside — as a function of μ_1 for $\mu_2 = 0.2$ and $\mu_3 = 1$. (Here N actually refers to the number of primal modes and dual modes within our primal–dual formulation [4, 13, 19].) These results demonstrate the high accuracy of the RB prediction even for modest N; these results also demonstrate the importance of the error bounds not only in certifying the results but also in ensuring efficiency — permitting us to *safely* choose a small value of N without sacrificing accuracy or certainty. We note that for this unsteady problem we require larger N — since we must resolve the behavior in time as well, however the (Online) RB calculation (of both output and output error bound) is still $60\times$ (for $N = 25$) faster than the direct truth evaluation.

REFERENCES

[1] B. O. Almroth, P. Stern, and F. A. Brogan, 1978. "Automatic choice of global shape functions in structural analysis" *AIAA Journal* **16** pp. 525–528.
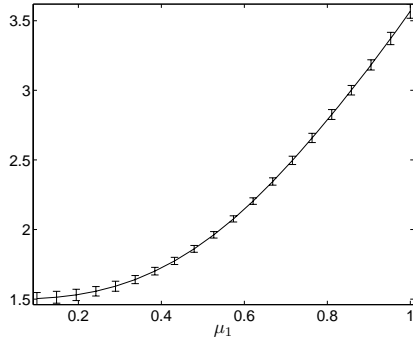
Figure 6. RB output and RB error bars — defined as the interval $[s_N(\boldsymbol{\mu}) - \Delta_N^s(\boldsymbol{\mu}), s_N(\boldsymbol{\mu}) + \Delta_N^s(\boldsymbol{\mu})]$ — as a function of μ_1 for $\mu_2 = 0.2$, $\mu_3 = 1$ and $N = 25$.

[2] V.S. Arpaci, 1966. *Conduction heat transfer*. Addison-Wesley , Reading, UK.

[3] S. Deparis, 2008. "Reduced basis error bound computation of parameter-dependent navier–stokes equations by the natural norm approach", *SIAM Journal of Numerical Analysis*, **46** (4), pp. 2039–2067.

[4] M. A. Grepl, A. T. Patera, 2005. "*A Posteriori* error bounds for reduced-basis approximations of parametrized parabolic partial differential equations". *M2AN (Math. Model. Numer. Anal.)* **39** (1), pp. 157–181.

[5] D. B. P. Huynh, G. Rozza, S. Sen, A. T. Patera, 2007. "A successive constraint linear optimization method for lower bounds of parametric coercivity and inf-sup stability constants", *C. R. Acad. Sci. Paris, Analyse Numérique* **345** (8), pp. 473–478.

[6] D. B. P. Huynh, C. N. Nguyen, G. Rozza, A. T. Patera, 2007-09, Documentation for rbMIT Software. http://augustine.mit.edu/methodology/ methodology_rbMIT_System.htm ©MIT, Tech. Lic. Office 12600, Cambridge, MA, US.

[7] A. M. Khounsary, *et al.*, 1998. "Heat Transfer Education:Keeping It Relevant and Vibrant". Proceedings of the ASME Heat Transfer Division (R.A. Nelson, Jr., et al. Eds.), HTD-Vol. 361-**3**/ PID-Vol. 3, pp. 17-24, ASME.

[8] N. C. Nguyen, G. Rozza, D. B. P. Huynh, A. T. Patera, 2009. "Reduced basis approximation and a posteriori error estimation for parametrized parabolic pdes; Application to real-time Bayesian parameter estimation". In *Computational Methods for Large Scale Inverse Problems and Uncertainty Quantification*. L. Biegler, *et al.*, (eds.), John Wiley and Sons, UK.

[9] N. C. Nguyen, G. Rozza, A. T. Patera, 2009. "Reduced basis approximation and a posteriori error estimation for the time-dependent viscous Burgers equation", *Calcolo*, in press.

[10] N. C. Nguyen, K. Veroy and A. T. Patera, 2005. "Certified real-time solution of parametrized partial differential equations". In *Handbook of Materials Modeling*, S. Yip (ed.), Springer, New York, pp. 1523–1558.

[11] A. K. Noor, J. M. Peters, 1980. "Reduced basis technique for nonlinear analysis of structures", *AIAA Journal*, **18** (4), pp. 455–462.

[12] T. A. Porsching, 1985. "Estimation of the error in the reduced basis method solution of nonlinear equations", *Mathematics of Computation*, **45** (172), pp. 487–496.

[13] C. Prud'homme, D. Rovas, K. Veroy, Y. Maday, A. T. Patera and G. Turinici, 2002, "Reliable real-time solution of parametrized partial differential equations: reduced-basis output bound methods", *Journal of Fluids Engineering*, **124** (1), pp. 70–80.

[14] A. Quarteroni, A. Valli, 1997. *Numerical Approximation of Partial Differential Equations*, 2nd ed., Springer-Verlag, Berlin.

[15] R. J. Ribando, L. G. Richards, G. W. O'Leary, 2004. " A "hands-on" approach to teaching undergraduate heat transfer". In Proceedings of IMECE2004, ASME, paper IMECE2004-61165, Anaheim, CA.

[16] R. J. Ribando, 2002. *Heat Transfer Tools*, McGraw-Hill, NY.

[17] R. J. Ribando, T. C. Scott, L. G. Richards, G. W. OLeary, 2002. "Using Software with Visualization to Teach Heat Transfer Concepts". In Proceedings of the 2002 American Society for Engineering Education Annual Conference and Exposition, Montreal, CA.

[18] P.C. Richmond, S. Lin, 2008. "Preliminary Testing of a .Net Based Educational Heat Transfer Simulator". In Proceedings of AIChe Annual Meeting, November 2008, Philadelphia, PA.

[19] G. Rozza, D. B. P. Huynh, A. T. Patera, 2008. "Reduced basis approximation and a posteriori error estimation for affinely parametrized elliptic coercive partial differential equations: Application to transport and continuum mechanics", *Archives Computational Methods in Engineering*, **15** (3), pp. 229–275.

[20] M. Starnes, 2002, *Development of Technical Bases for Using Infrared Thermography for Nondestructive Evaluation of Fiber Reinforced Polymer Composites Bonded to Concrete*. PhD thesis Massachusetts Institute of Technology.

[21] F. Stern, *et al.*, 2004. "Development of Hands-On CFD Educational Interface for Undergraduate Engineering Courses and Laboratories". In Proceedings of the 2004 ASEE Annual Conference and Exposition, Salt Lake City, UT, paper 1526.

[22] K. Veroy, A. T. Patera, 2005. "Certified real-time solution of the parametrized steady incompressible Navier-Stokes equations; Rigorous reduced-basis *a posteriori* error bounds", *International Journal for Numerical Methods in Fluids*, **47**, pp. 773–788.